Shear at Twin Domain Boundaries in $YBa_2Cu_3O_{7-x}$

W. A. Caldwell, N. Tamura,* R. S. Celestre, A. A. MacDowell, and H. A. Padmore
Advanced Light Source, 1 Cyclotron Road, Berkeley, California 94720, USA

T. H. Geballe and G. Koster
Department of Applied Physics, Stanford University, Stanford, California 94305, USA

B. W. Batterman
Advanced Light Source, 1 Cyclotron Road, Berkeley, California 94720, USA
Stanford Synchrotron Radiation Laboratories, P.O. Box 4349, Stanford, California 94309, USA

J. R. Patel
Advanced Light Source, 1 Cyclotron Road, Berkeley, California 94720, USA
Department of Materials Science & Engineering, Stanford University, Stanford, California 94305, USA
(Received 3 June 2003; published 28 May 2004)

The microstructure and strain state of twin domains in $YBa_2Cu_3O_{7-x}$ are discussed based upon synchrotron white-beam x-ray microdiffraction measurements. Intensity variations of the fourfold twin splitting of Laue diffraction peaks are used to determine the twin domain structure. Strain analysis shows that interfaces between neighboring twin domains are strained in shear, whereas the interior of these domains are regions of low strain. These measurements are consistent with the orientation relationships of twin boundaries within and across domains and show that basal plane shear stresses can exceed 100 MPa where twin domains meet. Our results support stress field pinning of magnetic flux vortices by twin domain boundaries.

DOI: 10.1103/PhysRevLett.92.216105 PACS numbers: 68.35.Gy, 61.10.Nz, 74.72.Bk

Crystallographic transformation (polysynthetic) twins identified in bulk samples of $YBa_2Cu_3O_{7-x}$ (YBCO) [1] are common in YBCO films as well [2–4] and originate in the accommodation of the tetragonal to orthorhombic phase transition during postgrowth cooling. That twin boundaries can be effective vortex pinning centers in YBCO was revealed early on by magnetic hysteresis experiments on the same single crystal in the twinned and untwinned states [5]. Subsequently, the anisotropic pinning behavior measured in monodomain single crystals [6,7] and films [8,9] showed that twin boundaries can channel flux motion parallel to the twin planes and pin perpendicular flux motion. The higher pinning strength of multidomained single crystals [7] and films [9,10] relative to monodomain material has been attributed both to the geometrical blocking of vortex channeling by intersecting twin planes and to pinning by the local disorder at these intersections. However, the strain field at twin domain boundaries also seems a likely candidate for flux pinning because the marked effect of strain upon the superconducting properties of YBCO has been well documented. Strain has been cited as a factor in the decrease of critical currents across grain boundaries [11], in the modification of the critical temperature T_c in thin films [12–14], and as a flux-pinning mechanism induced by lattice mismatch [15].

Twinning in YBCO takes place across the basal diagonals of the orthorhombic unit cell leading to four uniquely oriented twin lattices [1,16]. As imaged by transmission electron microscopy (TEM), twins primarily occur in domains consisting of pairs of orientations twinned across either (110) or $(1\bar{1}0)$ [17,18]. Twin lattices within a domain meet at a mutual twinning plane and have perfect lattice registry so that they are coherent and the domain interior is strain free; however, orthorhombic symmetry disrupts lattice registry across domain boundaries so that domain interfaces will be strained [19,20]. While strain contrast of such interfaces has been imaged by TEM [17,21], the strain associated with them has not been measured.

In this Letter, we present a synchrotron white-beam x-ray microdiffraction study of *c*-axis YBCO films supported by $SrTiO_3$ (STO) substrates. White-beam diffraction patterns were collected from submicron sized areas in a step by step scanning method, allowing us to determine the spatial variation of the twinning microstructure and strain. Our results show that the partitioning of the film into twin domains is clearly correlated with the distribution of basal shear strain, consistent with the relative orientations of twin boundaries both within and across domains. Finally, the relevancy of our findings to flux pinning by twins is presented.

Our samples are 260 nm thick YBCO films on a (001)-STO substrate. Films were made by pulsed laser deposition at 810 °C in an ambient oxygen atmosphere and postgrowth oxygenated at 420 °C for 1 h prior to removal from the growth chamber. Resistivity vs temperature measurements indicated the samples were of

good quality with a critical temperature T_c of 90 °K. Oxygen content and stress-free lattice parameters of the YBCO film were determined from established relations with T_c [22] indicating a high oxygen content ($x < 0.1$) with $a = 3.815$ Å, $b = 3.889$ Å, and $c = 11.676$ Å.

X-ray diffraction measurements were taken at room temperature using the x-ray microdiffraction beamline (7.3.3) at the Advanced Light Source in Berkeley, CA [23]. An intense polychromatic x-ray microbeam (0.8×0.8 mm) was produced by focusing x rays coming from a synchrotron bend magnet source via a pair of elliptically bent Kirkpatrick Baez mirrors. X-ray Laue patterns were collected in reflection mode by a large area charge coupled device (CCD) detector (Bruker SMART6000). Laue patterns were indexed and analyzed to provide the deviatoric strain state of each of the four twins by comparing peak positions to their ideal unstrained positions. Variations in peak intensity across the sample were used to determine the twinning microstructure.

Figure 1 shows a typical diffraction pattern taken from our sample. Experimental geometrical parameters (sample-detector distance, center channel position, and tilts of detector with respect to beam) were determined by using the STO substrate as an unstrained reference. The brightest reflections in the pattern are due to the STO substrate, while the remaining peaks are from the film. A few of the more intense YBCO reflections are indexed in the figure. The YBCO peaks (inset of Fig. 1), unlike the simple STO peaks, are split due to the superposition of diffraction patterns from the four suborientation twin states S_1^+ and S_2^- twinned across $(1\bar{1}0)$ and S_1^- and S_2^+ twinned across (110) (notation after Ref. [19][19]).

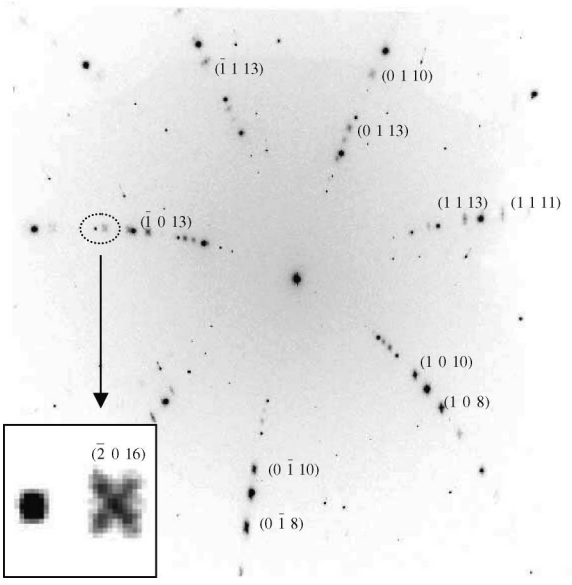

FIG. 1. White beam Laue diffraction pattern of YBCO film on STO substrate taken with a 10-second exposure. Miller indices of a few YBCO reflections are shown. Inset shows enlargement of a STO peak (left) and a YBCO peak (right).

Figure 2 shows a comparison of the experimental and model reciprocal lattice for twinned YBCO. Indexation of the diffraction pattern provided the exact orientation matrix of the sample with respect to the laboratory basis, which was then used to project each pixel of the CCD frame into the q-space (reciprocal space) coordinates of the unit cell basis shown in Fig. 2(a). This q-space projection, shown in Fig. 2(a) for peaks of type (h k 13), is thus free from any artifacts due to the experimental geometry. For comparison, Fig. 2(b) shows a schematic of the four twin reciprocal lattice orientations at a slice normal to $\mathbf{c}^*$ overlaid on the tetragonal reciprocal lattice. Epitaxial YBCO films deposited on (001)-STO substrates maintain an alignment of $\langle 110 \rangle$ between film and substrate during the orthorhombic to tetragonal transition, at the expense of alignment along $\langle 100 \rangle$ and $\langle 010 \rangle$ [24]. Both real diffraction pattern and model reciprocal lattice show that the fourfold lattice splitting produces Laue peaks that have a shape dependent upon Miller indices. This reciprocal lattice construction is crucial to indexation, determination of twin distribution, and strain analysis as will be discussed later.

The width and position of peaks in Fig. 2 yield information about twin size and degree of orthorhombicity. X-ray peak broadening measurement is a classical nondestructive method of determining crystal size. Average twin size (t) is determined from the wavelength (λ) of the Laue reflection, angular width (B) of the peak, and the Bragg diffraction angle (θ_b) using the Scherrer equation:

$$t = 0.9\lambda / B \cos\theta_b. \quad (1)$$

An angular profile along the path indicated on the $(\bar{2}\ 0\ 13)$ peak [presented in lieu of the (0 0 13) peak] in Fig. 2(a) was used to determine the width of one twin from each of the twinning systems. The average peak full width at half maximum of 0.34° yielded, after using a neighboring STO substrate peak to determine instrumental broadening, a value of approximately 50 nm, similar to twin size observed in other thin films of YBCO by TEM [16]. Thus, our 1 μm x-ray beam averages over approximately 20 twins in each diffraction exposure. The positions of the $(\bar{2}\ 0\ 13)$ peak in Fig. 2(a) give a b/a ratio of 1.013, in reasonable agreement with the theoretical value of 1.019 using a and b determined from the T_c measurements [the b/a ratio in Fig. 2(b) was increased to 1.127 for the sake of clarity].

The unique ability of synchrotron based Laue x-ray microdiffraction to completely characterize the reciprocal space lattice with a single 10-second exposure allowed us to determine the spatial distribution of microstructure and strain in a manageable time frame. We used variations in the intensities of the split Laue peaks as a proxy for the relative representation of each twin orientation, as in previous studies of YBCO twins using a conventional monochromatic x-ray source [25].

Partitioning of the sample into domains consisting of twin pairs is evident upon inspection of the high-order

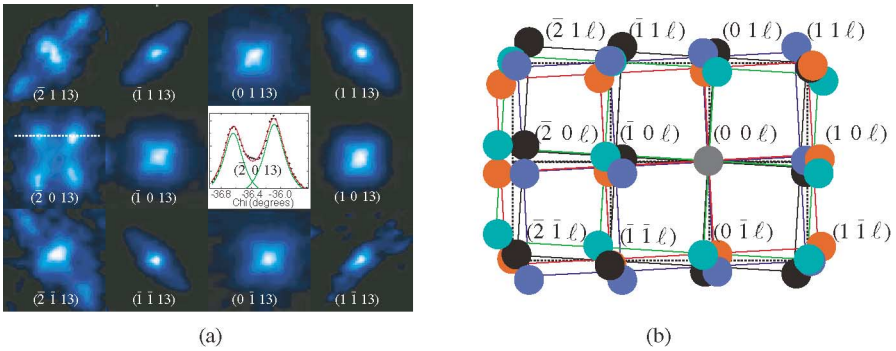

FIG. 2 (color). (a) Q-space projection of (h k 13) layer reflections. Each box spans 0.02 Å^{-1} on a side. Also shown is an angular profile through the ($\bar{2}$ 0 13) reflection along the path indicated by the dashed white line. (b) Reciprocal space lattice decorated by the four {110} twins: S_1^+ (red), S_1^- (green), S_2^+ (blue), and S_2^- (black). Tetragonal phase reciprocal lattice shown with dashed frame.

clover shaped Laue reflections of the types (h 0 l) and (0 k l) as shown for the ($\bar{2}$ 0 11) peaks from a (110) domain [Fig. 3(a)] and boundary region [Fig. 3(b)]. The diffraction signal for (110) twins in Fig. 3(b) originates from areas of the domain in close proximity to the (1$\bar{1}$0) domain, i.e., near the domain boundary. A profile in q space through the S_1^- and S_2^+ diffraction peaks [solid line in Fig. 3(a)] in Fig. 3(c) shows a shift in peak positions accompanying the fall in intensity going from a (110) domain to the domain boundary. The solid lines in Fig. 3(c) were obtained using a multiple Lorentzian peak fit routine to the individual twin peaks, and the peak maxima obtained from these fits are indicated by vertical markers. We note a subtle, yet measurable, inward peak shift of

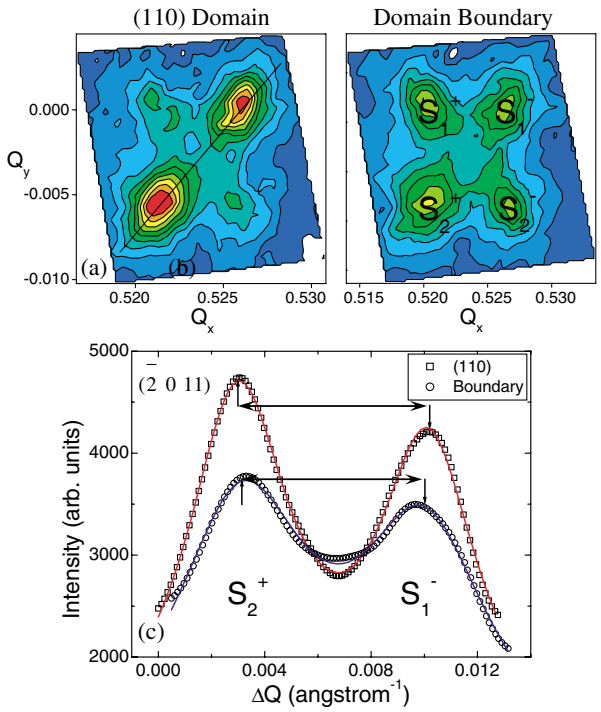

FIG. 3 (color). Q-space projection of ($\bar{2}$ 0 11) peaks from (a) (110) domain and (b) domain boundary region. Twin orientations labeled in (b). Profiles through the S_1^- and S_2^+ peaks (solid line) plotted in (c) for the (110) domain (squares) and boundary region (circles). Distance between S_1^- and S_2^+ peaks indicated by arrows that span the fitted peak positions (vertical markers).

~4% between the (110) peaks near the domain boundary and the (110) domain far from it, indicating that these boundary regions are strained.

Complete strain analysis of the white-beam Laue patterns entailed determining the deviation of each peak position from its ideal unstrained position. The resulting deviatoric strain tensor describes the change in the shape of the unit cell from its unstrained state. We used only well-resolved, high-order peaks and disregarded those with intrinsic overlap from other twins (e.g., central peaks of {11l} reflections) or the substrate. The 15–20 unique peaks per twin selected in this way enabled us to determine the deviatoric (nondilatational) strain state with an accuracy determined from a statistical procedure as well as estimated from the relation $\varepsilon = (\Delta d/d) = \cot\theta\Delta\theta$. The pixel resolution and specimen to camera distance give $\Delta\theta \approx 0.02°$, which when combined with a Bragg angle of 45° yields a strain sensitivity $\varepsilon \approx 3 \times 10^{-4}$.

Figure 4 shows a mosaic of ($\bar{2}$ 0 16) diffraction spots for a scan of a 10 × 10 μm area. Most of the images show diffraction from both twin sets, indicating that the beam is sampling areas of domain boundaries. Yellow lines are drawn to show where the intensity of both twin sets are equal. Regions where one twin set dominates indicate domain interiors and are seen at upper left for a (110) domain and at bottom right for a (1$\bar{1}$0) domain. Strain near the domain boundaries increases to values approaching -1.75×10^{-3}, a value almost 3 times that in the domain interiors. Measurements of strain for the other twins yielded shear values of similar magnitude, and other regions in the sample showed the same general behavior. Using the elastic constants of YBCO [26], we determined that the basal shear stresses corresponding to the measured strains exceed 100 MPa at the domain interfaces.

High resolution electron micrographs of twin domain boundaries show obvious distortion of the atomic planes at twin domain boundaries, but fail to establish the presence of any dislocations in these regions [21]. Thus, any elementary ideas based on a simple Burgers model of a small angle tilt (dislocation) boundary cannot be used to describe or evaluate the strain due to these twin boundaries. In a detailed study of twin formation and interaction in YBCO, Wadhawan [19] concluded that since the (110)

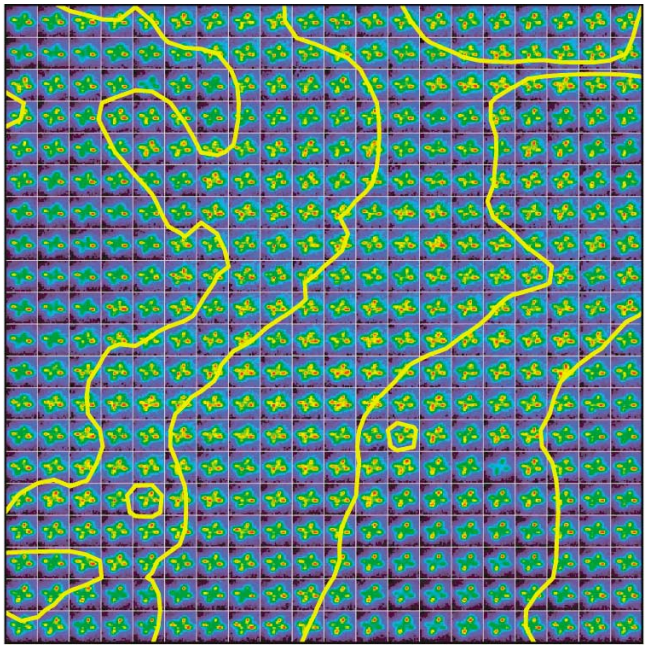

FIG. 4 (color). Mosaic of $(\bar{2}\,0\,16)$ diffraction spots taken from 10×10 μm area. Yellow lines drawn where intensity of twin domains are equal. Regions where one twin set dominates indicate domain interiors and are seen at upper left for a (110) domain and at bottom right for a $(1\bar{1}0)$ domain. Most of the mosaic images show diffraction from both twin sets, indicating that the beam is sampling areas of domain boundaries.

and the $(1\bar{1}0)$ twin states nucleate and grow independently there are many regions in the crystal where their respective domains intersect. Violation of long range translational periodicity in these regions gives rise to strain fields whose effect "is felt at distances far greater than the typical thickness of the twin walls." Indeed, our results confirm that domain boundaries are the regions where the measured strain is greatest.

Strain due to thermal mismatch between film and substrate is negligible because above ~10 nm the film is substantially relaxed [14,25,27], with lattice parameters close to bulk values. Our 260 nm film is much thicker than the critical thickness, so we expect it to be minimally strained due to thermal mismatch. In any case, thermal mismatch strain would be homogeneously distributed and not give the spatial variation demonstrated here.

The basal shear strain is a measure of the distortion of the YBCO *a-b* plane containing the Cu-O sublattice thought to be important for superconductivity. Deviation of the lattice from its equilibrium configuration at domain boundaries means that this region will be the most prone to revert to the normal, nonsuperconducting, state and preferentially trap magnetic flux. Here we have provided evidence that twin domain boundaries intrinsically produce a strain field likely to be important in pinning flux vortices.

The Advanced Light Source is supported by the Director, Office of Science, Office of Basic Energy Sciences, Materials Sciences Division, of the U.S. Department of Energy under Contract No. DE-AC03-76SF0098 at Lawrence Berkeley National Laboratory. The authors thank Intel Corp. for partial funding of the end station and G. Daniels and D. C. Larbalestier for contributing samples. The research at Stanford was supported by the AFOSR.

*Email address: NTamura@lbl.gov

[1] G. J. McIntyre, A. Renault, and G. Collin, Phys. Rev. B **37**, 5148 (1988).
[2] N. Didier *et al.*, J. Alloys Compd. **251**, 322 (1997).
[3] J.-L. Maurice *et al.*, Thin Solid Films **319**, 211 (1998).
[4] D. Schweitzer *et al.*, Thin Solid Films **280**, 147 (1996).
[5] U. Welp *et al.*, Appl. Phys. Lett. **57**, 84 (1990).
[6] J. Z. Liu *et al.*, Phys. Rev. Lett. **66**, 1354 (1991).
[7] M. Oussena *et al.*, Phys. Rev. B **51**, 1389 (1995).
[8] C. Villard *et al.*, Phys. Rev. Lett. **77**, 3913 (1996).
[9] D. G. Crété *et al.*, Physica (Amsterdam) **372C**, 634 (2002).
[10] S. Berger *et al.*, Phys. Rev. B **63**, 144506 (2001).
[11] M. F. Chisholm and S. J. Pennycook, Nature (London) **351**, 47 (1991).
[12] M. Salluzzo *et al.*, Phys. Rev. B **66**, 184518 (2002).
[13] H. Y. Zhai and W. K. Chu, Appl. Phys. Lett. **76**, 3469 (2000).
[14] L. X. Cao *et al.*, Physica (Amsterdam) **337C**, 24 (2000).
[15] Y. Li and Z.-X. Zhao, Physica (Amsterdam) **351C**, 1 (2001).
[16] C. H. Chen, J. Kwo, and M. Hong, Appl. Phys. Lett. **52**, 841 (1988).
[17] G. Van Tendeloo *et al.*, Physica (Amsterdam) **167C**, 627 (1990).
[18] A. H. King and Y. Zhu, Philos. Mag. A **67**, 1037 (1993).
[19] V. K. Wadhawan, Phys. Rev. B **38**, 8936 (1988).
[20] I. M. Shmyt'ko and V. S. Shekhtman, in *The Real Structure of High-T_c Superconductors*, edited by V. S. Shekhtman (Springer, New York, 1993), Vol. 23, pp. 23–43.
[21] Z.-X. Cai and Y. Zhu, in *Microstructures and Structural Defects in High-Temperature Superconductors*, edited by Z.-X. Cai and Y. Zhu (World Scientific, Singapore, 1998), pp. 147–202.
[22] R. G. Munro and H. Chen, J. Am. Ceram. Soc. **79**, 603 (1996).
[23] N. Tamura *et al.*, Rev. Sci. Instrum. **73**, 1369 (2002).
[24] J. D. Budai, R. Feenstra, and L. A. Boatner, Phys. Rev. B **39**, 12 355 (1989).
[25] J. Brötz *et al.*, Phys. Rev. B **57**, 3679 (1998).
[26] H. Ledbetter and M. Lei, J. Mater. Res. **6**, 2253 (1991).
[27] J. Zegenhagen *et al.*, Solid State Commun. **93**, 763 (1995).